JCTC Journal of Chemical Theory and Computation

Density Functional Study of H−D Coupling Constants in Heavy Metal Dihydrogen and Dihydride Complexes: The Role of Geometry, Spin−Orbit Coupling, and Gradient Corrections in the Exchange-Correlation Kernel

Boris Le Guennic,[†] Serguei Patchkovskii,[‡] and Jochen Autschbach*,[†]

Department of Chemistry, 312 Natural Sciences Complex, State University of New York at Buffalo, Buffalo, New York 14260-3000, and Theory and Computation Group, Steacie Institute for Molecular Sciences, National Research Council Canada, 100 Sussex Drive, Ottawa, Ontario K1A 0R6, Canada

Received February 25, 2005

Abstract: The H−D nuclear spin−spin coupling constants J(H−D) of 14 heavy transition-metal dihydrogen and dihydride complexes were calculated with density functional theory using the "zeroth-order regular approximation" (ZORA) for the one-electron operators. The applied gradient-corrected density functional was able to achieve an average agreement with experimental data that is almost comparable to what has been obtained recently with hybrid functionals [*J. Am. Chem. Soc.* **2004**, *126*, 14249]. However, a systematic overestimation of J(H−D) for complexes with short H−D distances was obtained, which could be traced back to problems of the gradient functional to describe the H−D coupling in free dihydrogen well. We implemented gradient corrections for the exchange-correlation (XC) kernel and employed a basis sets with high-exponent 1s function for the coupled hydrogens. The gradient terms in the XC kernel turned out to be very important in order to achieve reasonable agreement with experimental coupling constants. On the other hand, our study reveals that spin−orbit relativistic corrections on the H−D coupling constants are comparatively small and need not to be considered at the accuracy level of currently available "standard" density functionals. The discussion of the results highlights the strong dependence of the coupling constants on the H−D distance and the possibility of large vibrational contributions to them. We also discuss the coupling constant for the hydrogen molecule in detail because of its relevance to the coupling in dihydrogen and dihydride complexes.

1. Introduction

A number of authors have pointed out the sensitivity of H−D nuclear spin−spin coupling constants with respect to the H−D distance in η^2-dihydrogen[1] and dihydride complexes of transition metals.[1−6] Of particular interest is the relationship between J(H−D) and the H−D distance. Its knowledge allows for estimating the H−D distance in such complexes in solution from NMR measurements of J(H−D). This has been recently emphasized again in ref 7. For instance, dihydrogen complexes can be classified as "elongated" based on solution NMR measurements. A recent example can be found in ref 8 which reported the synthesis and properties of iridium bis(phosphinite) pincer complexes. Elongated dihydrogen complexes afford H−H distances between 1.0 and 1.6 Å, whereas the H−H distance in true dihydrogen complexes is close to the 0.74 Å found for H_2 itself. Typically, H−H distances in dihydrogen complexes range from about 0.8 to 1.0 Å. Once the H−H distance increases to 1.6 Å, the complex is classified as a dihydride instead. From the shape of the potential energy surface (PES) in the H−H stretch region, Gelabert et al. have also identified

* Corresponding author e-mail: jochena@buffalo.edu.
[†] State University of New York at Buffalo.
[‡] National Research Council Canada.

10.1021/ct050042j CCC: $30.25
Published on Web 05/21/2005

"compressed dihydride" complexes. The classification depends on whether the deepest minimum of the PES of elongated complexes is rather in the dihydrogen or in the dihydride regime.[4] Due to the small mass of the hydrogen isotopes, the measured H−D coupling constant might be strongly influenced by stretching and bending motions of the H−Me−D subsystem. Thus, elongated dihydrogen and compressed dihydride complexes can be expected to exhibit different temperature dependence of J(H−D).[4]

Besides structural information for newly synthesized metal complexes, an important application of NMR measurements on complexated H_2 is related to the safe storage and handling of hydrogen, which represents one of the challenges for use of hydrogen in mobile energy generation.[12,15,17] In this context, nuclear magnetic resonance has established itself as one of the most powerful, nondestructive techniques for the analysis of structure, composition, and dynamics of guest molecules in microporous materials.[10,13] NMR spin−spin coupling constants provide a sensitive probe of the interactions of the H_2 guests with transition-metal centers in such systems, particularly because of their sensitivity to the H−H distance. As a result, NMR can be used to follow the transition between physisorption and chemisorption regimes in a hydrogen storage system. In such situations, first-principle calculations might permit discrimination between different possible structural interpretations of the experimental data.

From a theoretical/computational viewpoint, the prediction or verification of NMR parameters for transition-metal complexes, in particular with heavy metals, is not unproblematic.[20−23] The reason is the sensitivity of NMR parameters to internal and external influences. It is necessary to treat electron correlation, relativistic effects, but also the influence from the complexes' chemical environment (usually solvent molecules) simultaneously at a high level. Prior experience with density functional theory (DFT) calculations of metal chemical shifts has shown that hybrid functionals such as B3LYP perform quite well for 3d metals[24] (in particular for Fe chemical shifts[25] where nonhybrid DFT was shown to fail spectacularly). However, a reinvestigation of Fe shifts has recently shown that the hybrid DFT results might deteriorate in case this functional is used also for the geometry optimizations.[26] Ligand chemical shifts in metal complexes, on the other hand, are often well described at the nonhybrid DFT level. Similar conclusions were drawn for metal−ligand nuclear spin−spin coupling constants.[20]

Somewhat surprisingly, for spin−spin coupling constants between ligands in metal complexes there are only a few computational data available in the literature. For a survey of DFT studies published up to late 2003 we refer the reader to ref 20. Acceptable agreement with experimental results and, more importantly, the observed trends could, for example, be achieved in studies of two-bond P−P couplings in Cp*(L)M=PAr (M = Co, Rh, Ir, L = PR_3 or CO, Ar = Mes*)[27] and group VI metal carbonyl phosphines $M(CO)_4(PH_3)_2$ (M = Cr, Mo, W),[28,29] for the Si−H coupling constant in $(\eta^5\text{-}C_5H_5)(CO)_2MnHSiCl_3$,[30] for the three-bond C−C coupling in $[(NC)_5Pt-Tl(CN)]^-$,[31] and for H−D coupling in Os dihydride complexes.[32,33] So far, the small number of computational studies of ligand−ligand coupling constants in metal complexes does not permit the drawing of general conclusions as to which computational model generally performs best.

A first-principles computational study of η^2-dihydrogen complexes of Os(II) of the form $[\eta^2\text{-}H_2Os(NH_3)_4L]$ was carried out by Hush et al. already in 1994.[32] Hartree−Fock and MP2 methods were employed but neither did yield acceptable agreement with the experimentally observed trends for different ligands L. A follow-up study using DFT, on the other hand, was able to achieve a much improved agreement between theory and experiment,[33] though for some ligands L (Cl^-, acetate) sizable differences between the calculated and measured values of J(H−D) remained. The success of DFT was attributed to the treatment of electron correlation, which is certainly an important aspect in NMR calculations in general[34] and for transition-metal systems in particular.[20] More recent computational studies of J(H−D) in η^2-dihydrogen complexes can be found in refs 7, 3, and 4. A comparatively large number of complexes with different metals were optimized in ref 7 using the mPW1PW91 hybrid density functional. The same functional was applied in subsequent computations of nuclear spin−spin coupling constants. Good agreement with experimental data was obtained. The calculations also showed that the coupling constants for the most elongated systems have negative signs. All previous computational studies of H−D coupling constants were considered relativistic effects by using scalar relativistic effective core potentials (ECPs).

So far, the question of whether spin−orbit coupling at the metal center has any influence on J(H−D) has not been addressed, though such an influence might be important in particular for strongly elongated H−D bonds with concomitant small coupling constants. A part of the coupling could be mediated and influenced by the metal's valence orbitals in this case. Further, the influence of the density functional on the combined geometry optimization/coupling constant calculation is unclear. In the present work we address these issues. We have recently implemented gradient corrections for the exchange-correlation (XC) kernel in calculations of spin−spin coupling constants. Thus, we have in addition taken the opportunity to investigate the question of their importance in nuclear spin−spin coupling constant calculations as part of the present study. As it turned out, their influence is large for J(H−D) and improves the agreement with experiment and hybrid DFT calculations substantially for complexes with medium to large H−D internuclear distances.

This work is organized as follows: In section 2 we summarize the computational details. The results of our computations in comparison with experimental data and the computations of ref 7 are presented and discussed in section 3. We conclude this work with a short summary in section 4.

2. Computational Details

We have performed the computations for the present study with the spin−orbit relativistic DFT approach for nuclear spin−spin coupling constants developed by Autschbach and Ziegler[37,38] and implemented in the Amsterdam Density

Functional (ADF) program package.[41−43] It is based on the two-component zeroth-order regular approximate (ZORA) relativistic one-electron Hamiltonian.[39,40] DFT exchange-correlation contributions in the calculations are based on nonrelativistic density functional expressions evaluated with the relativistic electron density obtained from the ZORA Fock operator.

The spin−spin coupling constant within the relativistic ZORA formalism consists of four terms that we denote by Fermi-contact (FC), spin-dipole (SD), and the paramagnetic and diamagnetic orbital terms (OP and OD). As in previous work,[31,44−47] we have chosen the well-known nonrelativistic nomenclature[48,49] for the four terms because, first, they yield the respective FC, SD, OP, and OD terms of Ramsey's nonrelativistic theory in the nonrelativistic limit (speed of light $c \rightarrow \infty$), and, second, they can be interpreted in a similar way.[37,50] In most scalar relativistic calculations, we have omitted the expensive computation of the SD contribution after test calculations had shown that its magnitude is small for all complexes. The SD term has been included in all spin−orbit calculations since there it leads only to a marginal increase in computational time. The spin−orbit results also contain important cross terms between OP and FC and OP and SD, respectively.[44]

In ref 7, geometry optimizations of the metal−dihydrogen complexes were performed using the mPW1PW91 hybrid density functional which includes modified Perdew-Wang exchange and Perdew-Wang 91 correlation terms.[51−53] Relativistic corrections were included in the computations via a scalar relativistic effective core potentials (ECPs) for the metal. In the present work, we have employed these geometries. Additionally, geometry optimizations were carried out with the Vosko-Wilk-Nusair (VWN)[54] local density approximation (LDA) functional as well as with the Becke-Perdew (BP)[55,56] and the revised Perdew-Burke-Ernzerhof (revPBE)[57−60] generalized gradient approximated (GGA) density functionals. The NMR H−D spin−spin coupling constants have been computed using the same functionals in order to analyze the sensitivity of the results to approximations in the (nonhybrid) density functionals. We have also applied the "statistical average of orbital-dependent model potentials" (SAOP) Kohn−Sham potential[61] to the calculation of the NMR coupling constants. It has been previously designed for, and successfully applied to, excitation energies and frequency dependent response properties.[62−65] Poater et al. have subsequently reported that for a range of light-nucleus chemical shifts the SAOP potential shows considerable improvement over other nonhybrid potentials, such as VWN or BP.[66] Our own work on heavy-metal−heavy-metal nuclear spin−spin coupling constants as well as heavy nucleus chemical shifts has also shown marked improvements of results obtained with SAOP as compared to standard GGAs in some cases,[47] though not consistently so[67] (however, in the case where large disagreement between theory and experiment occurred it is unclear whether the discrepancies are due to the Kohn−Sham potential or neglected solvent effects and other more "chemical" influences).

In our original implementation of ZORA spin−spin coupling calculations[37,38] a LDA XC kernel was applied to evaluate the linear response of the Kohn−Sham DFT potential due to the Fermi-contact (FC) perturbation operator. The FC perturbation does not cause a density but just a spin-density response. Consequently, there is no Coulomb contribution in the response of the Kohn−Sham potential when using nonhybrid functionals. Major improvements for spin−spin coupling calculations might thus be expected from considering GGA terms in the XC kernel, in particular for coupling constants involving light atoms. For the present work, we have implemented such terms based on the revPBE functional. Evaluation of GGA contributions to the matrix elements of the DFT response kernel $\hat{k}[\rho^{(0)}; \rho^{(1)}]$ employed the standard symmetric expression[9] for the second variation of the exchange-correlation energy to yield

$$\begin{aligned}\langle\phi_i|\hat{k}[\rho^{(0)};\rho^{(1)}]|\phi_j\rangle = &\sum_{\gamma,\,\delta=\alpha,\beta}\int f_{\gamma,\delta}\phi^*_{i,\gamma}\phi_{j,\gamma}\rho^{(1)}_\delta + \\ &\sum_{\gamma,\,\delta=\alpha,\beta}\sum_{b=x,\,y,\,z}\int f_{\gamma,\delta b}\phi^*_{i,\gamma}\phi_{j,\gamma}\frac{\partial}{\partial b}(\rho^{(1)}_\delta) + \\ &\sum_{\gamma,\,\delta=\alpha,\beta}\sum_{a=x,\,y,\,z}\int f_{\gamma a,\delta}\frac{\partial}{\partial a}(\phi^*_{i,\gamma}\phi_{j,\gamma})(\rho^{(1)}_\delta) + \\ &\sum_{\gamma,\,\delta=\alpha,\beta}\sum_{a,b=x,\,y,\,z}\int f_{\gamma a,\delta b}\frac{\partial}{\partial a}(\phi^*_{i,\gamma}\phi_{j,\gamma})\frac{\partial}{\partial b}(\rho^{(1)}_\delta) \quad (1)\end{aligned}$$

Here, ϕ_i and ϕ_j are combined spatial and spin basis functions (molecular orbitals in the algorithm that we have implemented), with the spatial components corresponding to α and β spins given respectively by $\phi_{i,\alpha}$ and $\phi_{i,\beta}$. Further, $\rho^{(0)}$ is the unperturbed electron spin-density, and $\rho^{(1)}$ is the first-order response of the spin density. The α and β components are indicated by the subscripts α and β.

The quantities $f_{\gamma,\delta}$, $f_{\gamma,\delta b}$, $f_{\gamma a,\delta}$, and $f_{\gamma a,\delta b}$ are explicit functions of the unperturbed electron density and its Cartesian gradients. They are given by the corresponding derivatives of the exchange-correlation energy density $\rho\cdot\epsilon_{XC}[\rho]$, for example

$$f_{\gamma,\delta} = \frac{\partial^2(\rho\cdot\epsilon_{XC}[\rho])}{\partial\rho_\gamma\partial\rho_\delta} \quad (2)$$

Expression (1) has the practical advantage of requiring at most the first derivatives of the unperturbed densities, first-order densities, and the basis functions. As a consequence, it is straightforward to implement in any DFT code which already includes gradient-corrected exchange-correlation potentials. A computationally more efficient asymmetric expression,[19] which does not require derivatives of the basis functions, would be somewhat more difficult to implement.

The expressions for the derivatives $f_{\gamma,\delta}$, $f_{\gamma,\delta b}$, $f_{\gamma a,\delta}$, and $f_{\gamma a,\delta b}$ are XC functional-specific (and often quite lengthy). These expressions, together with the computer code used to evaluate them, were derived and implemented using a computer algebra system, as will be discussed elsewhere.[19]

Full geometry optimizations of all metal dihydrogen complexes were carried out employing valence triple-ζ Slater-type basis sets with polarization functions for all atoms (TZP) from the ADF basis set library. Inner shells up to, but not including 5spd and 6sp for W, Os, Re, and Ta and 4spd and 5sp for Ru and Nb, were kept as frozen cores. Inner shells up to 1s for C, N and O, 2p for P, and 3d for Br were also kept frozen in the geometry optimizations. All electron Slater-type basis sets with two polarization functions (TZ2P) were used for the computations of NMR spin−spin coupling constants. Since it turned out that the H−D coupling is very sensitive to the description of the FC term we have also carried out NMR calculations where the TZ2P basis for the two coupled hydrogens has been augmented with four additional high exponent 1s functions. The additional exponents were chosen as $\zeta_{max}{}^{1.4 \cdot n}$, $n = 1...4$, where ζ_{max} is the highest 1s exponent of the unmodified TZ2P basis. We will denote this locally dense basis by TZ2P+steep.

3. Results and Discussion

The Hydrogen Molecule. Before we present the computed results for our set of 14 transition-metal complexes, it is beneficial to discuss the calculated indirect spin−spin coupling constant for the hydrogen molecule itself. The experimental value for the *J*-coupling constant is 42.9 ± 0.1 Hz for the HD isotopomer,[68] which corresponds to a *reduced* coupling constant K(H−H) of $23.3 \cdot 10^{19} T^2 J^{-1}$. Further, this corresponds to a *J*-coupling of 279.5 Hz for H_2. Here, and throughout the rest of this paper we have used a factor of 1.844 to convert the reduced coupling in 10^{19} SI units to the HD coupling constant in Hz and a factor of 12.01 to convert from K to J for H_2. The conversion factor from J(H−D) to J(H−H) is 6.514. All values for K coupling constants quoted in the following are understood to be in 10^{19} SI units.

The calculated value for K of H_2 at the TZP/revPBE(LDA) density functional level (i.e. using the revPBE XC potential but the LDA kernel) is 32.8 when the SD term is excluded, and 33.0 when the SD term is included. These results are for the experimental equilibrium distance of 0.741 Å and do not change substantially when the TZP/revPBE optimized geometry of 0.747 Å is used instead (33.0 excluding the SD term, 33.2 when the SD term is included). Dickson and Ziegler have in 1996 reported a calculated value of 28.2 (excluding the SD term) obtained with the VWN LDA functional, the TZ2P basis set, and a finite-perturbation approach. The additional *d* polarization functions of the TZ2P vs the TZP basis are not the reason for the large difference between the Dickson and Ziegler value and our result. We obtain a TZ2P/revPBE(LDA) value of 33.0 at the experimental bond distance (SD excluded), which is just 0.2 larger than the result with the TZP basis. The main effect stems from the functional. Indeed, when calculating the H−D coupling with the VWN functional and the TZ2P basis instead, the computed value drops to 28.6 which compares well with the literature value of 28.2, taking into account that the finite-perturbation approach used by Dickson and Ziegler might have introduced some numerical errors.

The coupling constant for H_2 at the equilibrium H−H distance is largely caused by the FC mechanism. An improvement of the calculated results toward the experimental coupling constant can be obtained by adding additional high-exponent 1s basis functions to the Slater-type basis sets. It is well-known that such additional basis functions are necessary to correctly describe the response of the electron density to the FC perturbation. The highest 1s exponent in the TZ2P basis for H is 1.580. We have added four 1s functions with exponents of 6.070, 4.336, 3.097, and 2.212, respectively, to the TZ2P basis for H as well as five density fit functions with exponents between 4.4 and 23.8 (from now on referred to as "TZ2P+steep"). The coupling constants of 24.2 (VWN) and 26.9 (revPBE(LDA)) obtained with the TZ2P+steep basis agree much better with the experimental value of 23.3 than those obtained with the unmodified TZ2P basis. The agreement is best for the VWN functional, which is obviously due to some fortuitous error cancellation.

The influence of the LDA approximation in the revPBE-(LDA) result is large. With the XC kernel of the revPBE functional, we obtain reduced coupling constants of 36.5 (TZ2P) and 29.6 (TZ2P+steep) at the experimental internuclear distance instead; i.e., the GGA contributions in the XC kernel cause an increase of the coupling constant by 11 and 10%, respectively. Thus, our "best" nonhybrid DFT result obtained at the TZ2P+steep/revPBE level including gradient corrections in the XC kernel overestimate the experimental value by 27%.

We have averaged the coupling constant with the ground-state nuclear vibrational wave functions for H_2, HD, and D_2, respectively, that were calculated in a discrete variable representation (DVR)[70] based on the TZ2P+steep/revPBE potential curve, using an approach similar to one reported in ref 71. With 23 points we obtain zero-point vibration corrected reduced couplings of 31.3 for H_2, 31.1 for HD, and 30.9 for D_2, at the TZ2P+steep/revPBE level, i.e., an additional 5% increase over the equilibrium value of 29.9. The vibrational correction of $1.2 \cdot 10^{19} T^2 J^{-1}$ corresponds to 2.2 Hz for HD. This is in good agreement with a value of 2.8 Hz ($1.5 \cdot 10^{19} T^2 J^{-1}$) recently calculated by Ruden et al.[69] with the B3-LYP hybrid functional. Vibrational corrections of at least the same order of magnitude (percentage-wise) might be expected in the metal complexes.

Unfortunately, in ref 69, only the B3-LYP vibrational correction but not the HD coupling constant itself was tabulated. In 2002, Sychrovsky et al. reported equilibrium nuclear spin−spin coupling constants calculated at the hybrid functional level, with a B3-LYP value of 23.0 for K(H−H).[36] In the same paper, the B3PW91 functional yielded a coupling of 21.1. When subtracting the vibrational correction of ref 69 from the experimental value to obtain an empirical experimental equilibrium coupling of 21.8, the B3PW91 agrees with an experiment slightly better than B3-LYP. The authors of ref 36 have also investigated the influence of Hartree−Fock (HF) exchange in the hybrid functional on the coupling constant by replacing a fraction x of the BLYP XC potential with HF exchange. For H_2, values of 0.1, 0.5, and 0.9 for x lead to a change of the coupling constant by only $1.3 \cdot 10^{19} T^2 J^{-1}$, from 24.1 for $x = 0.1$ to 25.4 for $x = 0.9$. A TZ2P+steep/BLYP(LDA)

Table 1. Calculated J_{HD} in Dihydrogen Complexes Using the TZ2P+steep Basis Set for the Hydrogen Atoms Bonded to the Metal (in Hz)

				ref 7	
	dist.[a]	VWN	revPBE[b]	calc.	exp.
$WH_2(CO)_3(P^iPr_3)_2$ (**1**)	0.84	38.4	47.3	34.8	34
$[RuH_2Cp(CO)(PCy_3)]^+$ (**2**)	0.93	27.2	33.9	27.2	22.3
$[RuH_2Cp(dmpe)]^+$ (**3**)	0.99	24.4	29.8	24.6	22.1
$[RuH_2Cp^*(dppm)]^+$ (**4**)	0.98	27.4	33.6	25.2	22.3
$[OsH_2(en)_2(OAc)]^+$ (**5**)	1.28	9.5	9.7	6.8	9
$ReH_2Br_2(NO)(P^iPr_3)_2$ (**6**)	1.33	11.0	11.8	9.8	12.8
$[TaH_2Cp_2(P(OMe)_3)]^+$ (**7**)	1.64	3.0	2.1	0.4	1.5
$OsH_2Cl[CH(C_2H_4P^tBu_2)_2]$ (**8**)	1.63	0.6	−0.1	−0.1	0
$[IrH_3Cp(PMe_3)]^+$ (**9**)	1.71	3.3	3.3	2.4	3.9
$[IrH_3Cp^*(PMe_3)]^+$ (**10**)	1.74	2.9	2.9	2.0	3.3
NbH_3Cp_2 (**11**)	1.76	0.6	−0.2	−1.1	−0.9
TaH_3Cp_2 (**12**)	1.82	0.0	−1.0	−2.0	−1.5
$TaH_2Cp_2(BO_2C_6H_4)$ (**13**)	2.03	0.1	−0.5	−1.2	−0.9
$ReH_2(CO)(NO)(PMe_3)_2$ (**14**)	2.22	−0.1	−0.8	−1.0	−1.0

[a] d(H−D) in angstroms from ref 7. [b] With revPBE XC potential and kernel.

result calculated by us is 26.5, with an expected increase of roughly 3.0 when the correct BLYP XC kernel would be used instead. This leads to a rough estimate of 29.5 for $x = 0$. This might indicate that the difference between $x = 0$ and $x = 0.1$ is extremely vital to obtain results close to experiment and that choosing $x = 0.1$ instead of 0.0 leads to a very significant reduction of the H−H coupling by about 20−25%. The use of different basis sets (IGLO-III in ref 36 vs TZ2P+steep here) could lead to different results at $x = 0$. Regarding the basis set convergence for the FC term, it has previously been pointed out in ref 72 that the polarized Slater-type basis sets employed here (even without additional high-exponent functions) are quite well suited to give a faithful description of the FC mechanism. We did not attempt to reach complete convergence of the results with respect to the number of high-exponent functions on the hydrogens. The errors resulting from the approximations in the density functional, neglect of vibrational corrections, solvent effects, etc. in the calculations on the metal complexes (see below) are expected to outweigh improvements from a basis for the hydrogens that is better than the TZ2P+steep basis employed here.

Our ZORA relativistic method for spin−spin coupling constants is currently restricted to nonhybrid functionals. We have obtained essentially the same H−D coupling constants (based on the LDA XC kernel) when using gradient functionals other than revPBE. Thus, it should be kept in mind in the following sections that for all GGA calculations of J(H−D) in metal dihydrogen complexes a pronounced overestimation of J(H−D) might be expected for complexes with H−D distances near the H_2 equilibrium bond length of 0.741 and large H−D coupling constants.

Computational Results for 14 Dihydrogen Metal Complexes. Table 1 lists the calculated H−D J-coupling constants for 14 transition-metal complexes with experimentally determined H−D distances between 0.84 and 2.25 Å. The data were obtained at the scalar ZORA level with the TZ2P+steep basis, using the optimized geometries of ref 7.

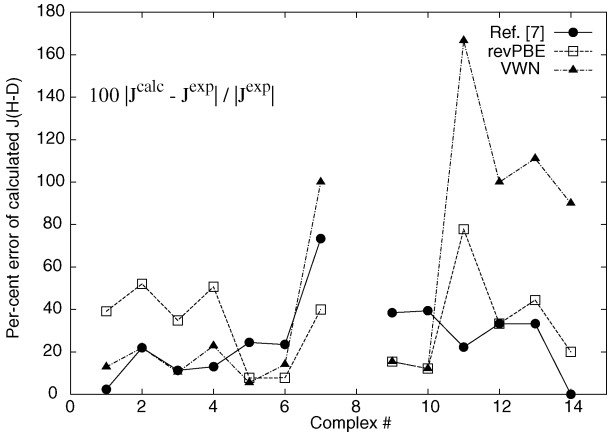

Figure 1. Relative deviations from experiment for the calculated H−D coupling constants obtained with the different methods listed in Table 1. See text for details. For complex **8**, the exp. value is 0.0; thus, no relative error is given. The lines were added to guide the eye.

Table 1 contains results obtained with the VWN and the revPBE functionals (both for XC potential and kernel).

Further, Table 1 lists the computational results of ref 7 which were obtained with a hybrid functional as well as the experimental coupling constants. The expected overestimation of J(H−D) for the complexes with short H−D distance is indeed visible in the revPBE results. One might take the fact that the calculated coupling in free hydrogen and in the dihydrogen complexes afford similar errors as an indication that the electronic structure of the H_2 moiety in complexes **1**−**4** is very similar to free H_2.

Whereas the calculated values using the VWN functional agree quite well with the experimental as well as with the hybrid functional data for the complexes **1**−**6** with short H−D distances, the accuracy of the VWN calculations deteriorates as d(H−D) increases. On the other hand, the revPBE results agree better with experiment for the elongated dihydrogen and the hydride complexes than for the complexes with short d(H−D).

For data sets such as the one in Table 1 where the elements differ by orders of magnitude, absolute unsigned differences do not allow for an easy comparison of different methods. For a small coupling constant, a deviation of 1 Hz would not be acceptable, whereas the same deviation would be considered acceptable or small for complexes where J(H−D) is of the order of 10 Hz. In Figure 1, we have therefore compared the relative unsigned errors of each computation.

The graphics reveals that the hybrid DFT method used in ref 7 performs best overall, even though some significant deviations between theory and experiment are visible. The largest relative deviations are obtained for the complexes with the largest H−H distances and the VWN functional. It should also be noted that the signs of the VWN results for these complexes do not agree with the revPBE and the hybrid DFT results (except for **14**; however, the calculated VWN value is much too small in magnitude). A disadvantage of using relative deviations is that they tend to inflate where the reference value is close to zero. Nevertheless, it can be

Table 2. Relative Deviation (in Percent) of the Computational Results of Table 1 from Experiment[a]

complex	Δ ref 7	Δ revPBE	Δ VWN	Δ revPBE[c]
1	2.4	39.1	12.9	38.8
2	22.0	52.0	22.0	45.7
3	11.3	34.8	10.4	18.6
4	13.0	50.7	22.9	42.6
5	24.4	7.8	5.6	31.1
6	23.4	7.8	14.1	43.8
7	73.3	40.0	100.0	0.0
8[b]				
9	38.5	15.4	15.4	17.9
10	39.4	12.1	12.1	18.2
11	22.2	77.8	166.7	44.4
12	33.3	33.3	100.0	20.0
13	33.3	44.4	111.1	33.3
14	0.0	20.0	90.0	20.0
average	25.9	33.5	52.5	28.8
median	23.4	34.8	22.0	31.1

[a] Mean unsigned relative deviation Δ calculated as $\Delta = 100|J^{calc} - J^{exp}|/|J^{exp}|$. [b] For complex **8**, the exp. value is 0.0; thus, no relative error is given. [c] For geometry optimized with the revPBE functional. See Table 6.

seen that the hybrid functional of ref 7 and the revPBE functional used here yield absolute deviations from experiment that decrease along with a decrease of the coupling constants' magnitudes. Hence, the accuracy does not deteriorate for complexes with large H−D distances (as seen in the relative deviations) and meaningful calculations are possible over the whole range of distances.

The good agreement between revPBE and hybrid DFT regarding the negative signs of the coupling constants for complexes **11**−**14** strongly supports the tentative conclusion of ref 7 that these coupling constants are negative. We will see later that the sign is not affected by the inclusion of spin−orbit coupling.

The deviations between calculated and experimental H−D couplings relative to the experimental value that are displayed in Figure 1 are collected in Table 2 (the last column is for revPBE optimized geometries which will be discussed later).

The median deviation for the VWN functional is small and does not reflect the poor overall performance of this functional. The small median stems from its good performance for the complexes with short d(H−D). The fact that the median and the average are very different indicates that the VWN functional causes a lot of outliers with large deviations from experiment. For the other two methods, the average and median agree well. The somewhat worse performance of the GGA functional compared to the hybrid is seen to result mainly from the overestimation of J(H−D) at short H−D distances that was also found for free H_2. For complex **8**, no relative error is listed because the experimental value is 0.0 Hz. Both the hybrid and the revPBE functional perform equally well for this complex whereas VWN is far off.

It should be noted that the equilibrium coupling constants (i.e. at R_e(H−H)) are not expected to agree well with the experimental values even at low temperature in case the PES is very anharmonic or in case the coupling constant surface has a large curvature around the equilibrium geometry. A recent paper has shown that for the complex [Cp*Ir(dmpm)-H_2]$^{2+}$, d(H−D) might be strongly temperature dependent and that the PES is indeed very anharmonic regarding the H−D stretching motion.[3] Increasing the temperature would lead to a shortened average H−D distance and thus likely to larger coupling constants. The opposite behavior might occur as well, depending on the shape of the PES and the *J*-coupling surface. Thus, the deviations displayed in Table 2 do not truly reflect the ability of the computations to accurately predict solution measurements at room temperature (for which solvent effects might also be important). The calculations afford systematic deviations from experiment due to the missing vibrational corrections. It might be the case that for the complexes with a significantly weakened, but still intact, H−D bond (i.e. for the elongated dihydrogen complexes) the magnitudes of the vibrational corrections *relative* to the equilibrium coupling constants are significantly larger than for the hydrogen molecule itself.

The Influence of Spin−Orbit Coupling on the H−D Coupling Constants. Table 3 lists computed results including the SD mechanism and/or spin−orbit coupling induced mechanisms on the H−D coupling, most notably from the FC/OP cross term. Included are also indirect effects on the FC, SD, OP, and OD mechanisms due to the change on the molecular orbitals when spin−orbit coupling is included variationally in the calculation. Most of the spin−orbit calculations have been carried out with the VWN functional and the TZ2P basis but without the additional steep functions. The scalar ZORA BP and SAOP calculations presented in Table 3 have been performed with the same basis. They are provided in order to demonstrate the influence of omitting the steep functions on the hydrogens in the coupling constant calculations (by comparison with Table 1) and to allow, for a select case, to verify that the magnitude of the spin−orbit contributions are the same in LDA and GGA calculations. All results were obtained using the optimized geometries of ref 7.

It is clear from the results that neither the inclusion of the SD term nor the inclusion of spin−orbit coupling causes dramatic changes to the H−D coupling constants. The changes to J(H−D) are 0.1 Hz in magnitude throughout the test set. Obviously, for coupling constants near zero, 0.1 Hz represents a substantial change. However, upon inspection of the results it can be seen that the VWN results for complexes with large H−D distances are still far off from experiment. Neither inclusion of spin−orbit coupling and/or the SD term would reconcile theory and experiment at the VWN level.

From these results we conclude that at the present level of accuracy (i.e. when considering the differences between theory and experiment) for local density functionals, gradient functionals, and hybrid functionals, relativistic spin−orbit corrections to the H−D coupling constant are not particularly significant, i.e., their negligence does not represent a major source of error in the computations. For more accurate computations that would deliver an accuracy of the order of 0.1 Hz it will be necessary to include all spin−orbit coupling effects. However, though highly accurate ab initio methods

Table 3. Calculated J_{HD} (in Hz) in Dihydrogen Complexes Using Optimized Geometries from Ref 7

		VWN	Becke-Perdew	SAOP
$WH_2(CO)_3(P^iPr_3)_2$	scal.	44.4	49.8	50.9
(**1**) *(0.89[a] − 0.84[b])*	scal.[c]	44.3		
	scal.[f]	41.1		
	s.o.	44.3		
$[RuH_2Cp(CO)(PCy_3)]^+$	scal.	28.8	32.7	32.9
(**2**) *(0.97[a] − 0.93[b])*	scal.[c]	28.7		
	s.o.	28.7		
$[RuH_2Cp(dmpe)]^+$	scal.	24.2	26.4	27.3
(**3**) *(1.02[a] − 0.99[b])*	scal.[c]	24.1		
	s.o.	24.1		
$[RuH_2Cp^*(dppm)]^+$	scal.	28.0	31.4	31.9
(**4**) *(1.10[d] − 0.98[b])*	scal.[c]			
	s.o.	28.0		
$[OsH_2(en)_2(OAc)]^+$	scal.	8.4	8.8	9.4
(**5**) *(1.34[d] − 1.28[b])*	scal.[c]	8.5		
	s.o.	8.6		
$ReH_2Br_2(NO)(P^iPr_3)_2$	scal.	9.9	10.4	11.0
(**6**) *(1.27[a] − 1.33[b])*	scal.[c]	10.0		
	s.o.	10.0		
$[TaH_2Cp_2(P(OMe)_3)]^+$	scal.	2.4	2.0	2.0
(**7**) *(1.67[a] − 1.64[b])*	scal.[c]	2.4		
	s.o.	2.4		
$OsH_2Cl[CH(C_2H_4P^tBu_2)_2]$	scal.	0.4	0.2	0.2
(**8**) *(1.57[e] − 1.68[a] − 1.63[b])*	scal.[c]	0.5		
	s.o.			
$[IrH_3Cp(PMe_3)]^+$	scal.	2.9	3.1	3.4
(**9**) *(1.69[d] − 1.71[b])*	scal.[c]	3.0		
	s.o.	3.0		
$[IrH_3Cp^*(PMe_3)]^+$	scal.	2.6	2.7	3.0
(**10**) *(1.73[a] − 1.74[b])*	scal.[c]	2.6		
	s.o.	2.7		
NbH_3Cp_2	scal.	0.4	0.1	0.2
(**11**) *(1.76[e] − 1.76[b])*	scal.[c]	0.4		
	s.o.	0.4		
TaH_3Cp_2	scal.	−0.4	−0.8	−0.8
(**12**) *(1.85[d] − 1.82[b])*	scal.[c]	−0.4	−0.7	−0.7
	s.o.	−0.4	−0.8	−0.8
$TaH_2Cp_2(BO_2C_6H_4)$	scal.	−0.1	−0.2	−0.3
(**13**) *(2.3[e] − 2.03[b])*	scal.[c]	−0.1		
	s.o.	−0.1		
$ReH_2(CO)(NO)(PMe_3)_2$	scal.	0.0	−0.1	−0.1
(**14**) *(2.25[a] − 2.22[b])*	scal.[c]	0.0		
	scal.[f]	0.0		
	s.o.	0.1		

[a] d(H−D) measured by solid-state NMR. See ref 7 and references therein. [b] d(H−D) obtained by DFT. [c] Including SD term. [d] d(H−D) measured by single-crystal neutron diffraction.[7] [e] d(H−D) measured by X-ray diffraction.[7] [f] TZP basis instead of TZ2P.

exist for calculations of spin−spin coupling, reproducing the experimental value to such accuracy would be a formidable task since there are many influences (solvent, temperature) in addition to electron correlation that would need to be considered also.

A comparison between the revPBE and the SAOP results shows that the SAOP potential does not improve upon the revPBE functional. In particular, it also yields the strong overestimation of J(H−D) at short H−D distances. Both the revPBE and SAOP results in Table 3 were calculated using the LDA XC kernel since a XC kernel consistent with the SAOP potential is not yet available. Thus, only the difference in the shapes and energies of the unperturbed molecular orbitals in the revPBE and SAOP calculations, respectively, is responsible for the slightly different J(H−D) when comparing the two methods. Whether both methods would yield similar results also if the respective XC kernels were employed in the calculations is unclear.

Table 4. Calculated J_{HD} in Dihydrogen Complexes Using the revPBE Functional with and without GGA Corrections in the XC Kernel (in Hz)[c]

	dist.[a]	revPBE(LDA)	revPBE
$WH_2(CO)_3(P^iPr_3)_2$ (**1**)	0.84	50.5	53.6
$[RuH_2Cp(CO)(PCy_3)]^+$ (**2**)	0.93	33.0	35.9
$[RuH_2Cp(dmpe)]^+$ (**3**)	0.99	27.3	29.6
	1.08[b]	23.3	25.3
$[RuH_2Cp^*(dppm)]^+$ (**4**)	0.98	31.7	34.1
$[OsH_2(en)_2(OAc)]^+$ (**5**)	1.28	8.7	8.6
$ReH_2Br_2(NO)(P^iPr_3)_2$ (**6**)	1.33	10.4	10.3
$[TaH_2Cp_2(P(OMe)_3)]^+$ (**7**)	1.64	2.0	1.3
$OsH_2Cl[CH(C_2H_4P^tBu_2)_2]$ (**8**)	1.63	0.2	−0.4
$[IrH_3Cp(PMe_3)]^+$ (**9**)	1.71	3.1	2.9
$[IrH_3Cp^*(PMe_3)]^+$ (**10**)	1.74	2.7	2.5
NbH_3Cp_2 (**11**)	1.76	0.0	−0.7
TaH_3Cp_2 (**12**)	1.82	−0.8	−1.5
$TaH_2Cp_2(BO_2C_6H_4)$ (**13**)	2.03	−0.3	−0.7
$ReH_2(CO)(NO)(PMe_3)_2$ (**14**)	2.22	−0.1	−0.5

[a] d(H−D) in angstroms from ref 7. [b] Optimization with the GGA revPBE functional. [c] Calculations based on geometries from ref 7, TZ2P basis.

The Influence of the GGA XC Kernel. In Table 4, calculated results at the revPBE(LDA) and the full revPBE level (where the XC kernel is consistent with the potential) are compared. Again, the TZ2P basis without the additional steep functions and the geometries from ref 7 have been used for this comparison.

As might have already been expected from the preceding discussion of the H_2 molecule, the influence of the GGA corrections in the XC kernel is sizable. For the short H−D distance dihydrogen complexes the increase in J(H−D) worsens the agreement with experiment, but this can be traced back to the problem of calculating H_2 itself. In particular for the complexes with large H−D distances, the inclusion of the GGA corrections in the kernel systematically improves the agreement with experiment as well as with the hybrid functional data. For example, for complexes **13** and **14**, a decrease of J(H−D) of as much as 0.4 Hz is obtained. This number is to be compared to experimental values of −0.9 and −1.0 Hz, respectively. The GGA terms in the XC kernel are obviously highly important to obtain the correct H−D coupling constants for these complexes.

By comparing the results in Table 4 with those in Table 1, the influence of the addition of steep 1s functions in the hydrogen basis can again be seen. In several cases, the presence of these functions reduces the magnitude of the coupling constant but consistently so only for the complexes with the shortest H−D distances. There are many other examples where the magnitude is increased instead; therefore, a general trend cannot be observed. Apparently, "cross terms"

Table 5. Calculated J_{HD} in Optimized Dihydrogen Complexes (in Hz)[a]

					ref 7	
	dist.[b]	VWN	Becke-Perdew (LDA)[j]	SAOP (LDA)	calc.	exp.
$WH_2(CO)_3(P^iPr_3)_2$	0.87[g]	43.5	48.8	49.8	34.8	34
(**1**) *(0.89[c] − 0.84[d])*	0.92[h]	41.0	45.8	46.8	34.8	34
	0.86[i]	43.7	49.1	50.2	34.8	34
$[RuH_2Cp(CO)(PCy_3)]^+$	0.99[g]	26.5	30.1	30.4	27.2	22.3
(**2**) *(0.97[c] − 0.93[d])*	1.32[h]	12.0	13.2	13.8	27.2	22.3
	0.98[i]	27.2	30.9	31.2	27.2	22.3
$[RuH_2Cp(dmpe)]^+$	1.41[g]	8.4	9.1	9.6	24.6	22.1
(**3**) *(1.02[c] − 0.99[d])*	1.43[h]	8.4	9.0	9.5	24.6	22.1
	1.08[i]	20.7	23.2	23.6	24.6	22.1
$[OsH_2(en)_2(OAc)]^+$	1.40[g]	5.6	5.8	6.3	6.8	9
(**5**) *(1.34[e] − 1.28[d])*	1.37[h]	6.3	6.5	7.1	6.8	9
	1.40[i]	5.7	5.8	6.4	6.8	9
$ReH_2Br_2(NO)(P^iPr_3)_2$	1.48[g]				9.8	12.8
(**6**) *(1.27[c] − 1.33[d])*	1.48[h]	6.5	6.8	7.2	9.8	12.8
NbH_3Cp_2	1.78[g]	0.2	−0.2	0.0	−1.1	−0.9
(**11**) *(1.76[f] − 1.76[d])*	1.76[h]	0.6	0.3	0.4	−1.1	−0.9
	1.79[i]	0.1	−0.2	−0.1	−1.1	−0.9
TaH_3Cp_2	1.83[g]	−0.5	−0.9	−0.9	−2.0	−1.5
(**12**) *(1.85[e] − 1.82[d])*	1.80[h]	−0.2	−0.5	−0.5	−2.0	−1.5
	1.84[i]	−0.6	−0.9	−1.0	−2.0	−1.5
$ReH_2(CO)(NO)(PMe_3)_2$	2.21[g]	0.0	−0.1	−0.1	−1.0	−1.0
(**14**) *(2.25[c] − 2.22[d])*	2.16[h]	0.1	0.0	0.0	−1.0	−1.0
	2.22[i]	0.0	−0.1	−0.1	−1.0	−1.0

[a] The geometry optimizations have been performed with ADF. [b] d(H−D) in Å. [c] d(H−D) measured by NMR. [d] d(H−D) obtained by DFT. [e] d(H−D) measured by single-crystal neutron diffraction. [f] d(H−D) measured by X-ray diffraction. [g] Optimization with the GGA Becke-Perdew functional. [h] Optimization with the LDA VWN functional. [i] Optimization with the GGA rev-PBE functional. [j] (LDA) indicated the use of the LDA XC kernel in the calculation of the H−D coupling.

of varying sign occur between the basis size and the quality of the functional. The resulting effect on the H−D coupling constant is balanced by such competing effects.

To summarize this paragraph, we find that the GGA corrections in the XC kernel are much more important than spin−orbit effects for predicting the correct sign and magnitude of the H−D coupling constant in our samples. The changes in the coupling constants can amount to several times the coupling constant calculated without a GGA XC kernel for complexes with large H−D distances. They are still of the order of 10% for those complexes with the largest H−D couplings among our samples. Further improvement can obviously be obtained with a hybrid functional, which is not surprising taking their known good performance for couplings between light nuclei into consideration.[35,36] This result is in marked contrast to calculations of ligand chemical shifts and metal−ligand coupling constants in transition-metal systems, where often nonhybrid functionals were found to yield excellent agreement with experiment.[20]

The Influence of the Optimized Geometry and Other DFT Potentials. The large difference between the experimental (22.3 Hz) and the GGA coupling constant for complex **3** in Table 4 based on the optimized geometry of ref 7 suggests that the optimized geometry of the complexes might be a source of error. The question arises whether the performance of any of the density functionals might change if geometries are obtained in consistency with the spin−spin coupling calculations. A marked improvement for complex **3** upon optimization with the revPBE functional, as seen in Table 4, has motivated us to investigate this issue in more detail. For Table 5, we have optimized the geometries of the complexes with the VWN, the Becke-Perdew (BP), and the revPBE functional. The coupling constants listed in Table 5 were subsequently calculated with the TZ2P, using the VWN and the BP functionals as well as the SAOP potential (unfortunately, SAOP optimizations could not be carried out because of the lack of a SAOP energy expression). We have not optimized all complexes at all DFT levels but restricted the investigation to a representative subset. Table 6, on the other hand, lists results obtained for all complexes. The data are based on a consistent treatment at the revPBE level which includes the geometry optimization. The results of Table 6 were calculated with the TZ2P+steep basis and the revPBE XC kernel in order to facilitate a direct comparison with Table 1.

Table 6. Calculated J_{HD} in Dihydrogen Complexes Using the TZ2P+steep Basis Set for the Hydrogen Atoms Bonded to the Metal (in Hz), revPBE Optimized Geometries

			ref 7	
	dist.[a]	revPBE	calc.	exp.
$WH_2(CO)_3(P^iPr_3)_2$ (**1**)	0.86	47.2	34.8	34
$[RuH_2Cp(CO)(PCy_3)]^+$ (**2**)	0.98	32.5	27.2	22.3
$[RuH_2Cp(dmpe)]^+$ (**3**)	1.08	26.2	24.6	22.1
$[RuH_2Cp^*(dppm)]^+$ (**4**)	1.02	31.8	25.2	22.3
$[OsH_2(en)_2(OAc)]^+$ (**5**)	1.40	6.2	6.8	9
$ReH_2Br_2(NO)(P^iPr_3)_2$ (**6**)	1.47	7.2	9.8	12.8
$[TaH_2Cp_2(P(OMe)_3)]^+$ (**7**)	1.68	1.5	0.4	1.5
$OsH_2Cl[CH(C_2H_4P^tBu_2)_2]$ (**8**)	1.66	−0.3	−0.1	0
$[IrH_3Cp(PMe_3)]^+$ (**9**)	1.72	3.2	2.4	3.9
$[IrH_3Cp^*(PMe_3)]^+$ (**10**)	1.76	2.7	2.0	3.3
NbH_3Cp_2 (**11**)	1.79	−0.5	−1.1	−0.9
TaH_3Cp_2 (**12**)	1.84	−1.2	−2.0	−1.5
$TaH_2Cp_2(BO_2C_6H_4)$ (**13**)	2.04	−0.6	−1.2	−0.9
$ReH_2(CO)(NO)(PMe_3)_2$ (**14**)	2.22	−0.8	−1.0	−1.0

[a] d(H−D) in Å, optimized with the revPBE functional.

From the data in Table 5 one can see that, as one might expect, the calculated coupling constants are sensitive to changes in the geometries upon optimization. For the VWN functional it is known that it strongly overbinds but tends to yields quite accurate geometries. Thus, the VWN functional is often used for geometry optimizations along with subsequent energy or property calculations at formally more accurate DFT levels. However, for example for complexes **2** and **3**, and to some extent for **1**, the optimized H−D distances are much too long (more than 0.3 Å) as compared to the experimental values (from solid-state NMR measurements) and the hybrid DFT results of ref 7. For complex **3**, also the Becke-Perdew functional fails to predict the H−D distance correctly. For complex **3**, the overestimation of d(H−D) by the VWN and the BP functionals leads to an underestimation of J(H−D) by almost a factor of 3. On the other hand, in all cases the revPBE functional yields H−D

distances that are similar to the hybrid-DFT results of ref 7 and the experimental values. Both LDA and the BP functional work best for the solid state[60] or for "classical" bonds, while the PBE family (and particularly revPBE and RPBE) gives a somewhat better balance for weak(er) interactions (for an application to transition-metal structures see, e.g., ref 73). Because the structures of the dihydrogen/dihydride complexes are a compromise between several competing weak interactions, revPBE might be expected to be more reliable on general principles.

Our most consistent results at the gradient DFT level are obtained with the revPBE functional. This functional also appears to yield consistently reliable geometries for our samples, whereas the other nonhybrid functionals fail spectacularly in some cases. In Table 6 we have therefore collected the H−D coupling constants similar to Table 2 (i.e. including GGA corrections in the XC kernel as well as the TZ2P+steep basis for the coupled hydrogens) but with geometries optimized at the ZORA-revPBE level instead of using the geometries of ref 7. The relative deviations from experiment are listed in the last column of Table 2 along with the average and the median. The average and median deviation are lower than those in the "Δ revPBE" column. This indicates that better agreement with experiment is obtained for the geometries optimized with the revPBE functional, in particular for complexes with medium to large H−D distances. The problem of overestimating the free dihydrogen coupling is still visible in the complexes with short H−D distances. It should be kept in mind that our data set is small. Therefore, small differences in the averages are statistically not significant. The average is now comparable to the hybrid functional data of ref 7, but the median is still noticeably larger. In two cases the deviation from experiment increases strongly (complexes **5** and **6**). In fact, the change in the results due to the different geometry is larger than what the data in Table 2 suggest since the computed results now under—instead of overestimate the experimental value. The revPBE calculations now predict an equilibrium coupling constant similar to the hybrid-DFT results of ref 7. It is possible that the experimental H−D coupling constants of complexes **5** and **6** include large positive vibrational effects which would cause the calculated equilibrium values to deviate substantially from experiment.

4. Summary and Conclusions

For the H_2 molecule, the calculated nuclear spin−spin coupling constant including gradient corrections both in the potential and in the kernel is about 30% too large in comparison with experiment. Therefore, most of the complexes with short H−D distances are not so well described at the GGA DFT level and exhibit a similar overestimation of J(H−D). For complexes with larger H−D distances, however, good agreement with experiment can be achieved. It turns out that the gradient corrections in the XC kernel are sizable. They are vital for obtaining the correct sign and magnitude of J(H−D) for the complexes with the largest H−D distance.

With the VWN functional, on the other hand, good agreement with experiment is obtained for complexes with short d(H−D). However, this functional fails completely for the dihydride complexes and also leads to extremely poor geometries for some of the complexes. In some cases, the BP GGA functional also yields poor geometries.

The calculations of H−D coupling constants based on geometries that were optimized with the revPBE functional and that were including high exponent 1s functions for the coupled hydrogens as well as GGA corrections in the XC kernel agree best with experiment among the calculations performed in this study. The average relative unsigned deviation from experiment obtained with this approach is similar to the hybrid DFT results of ref 7. The median deviations are larger because of the systematic overestimation of J(H−D) for complexes with short H−D distances. We have traced this overestimation back to problems of the GGA functional to describe the coupling constant for the free hydrogen molecule.

Basis sets with additional high-exponent s-functions are required for a faithful description of the Fermi-contact coupling mechanism. It is the dominant term at short d(H−D), whereas the long-range coupling constants are determined by a sensitive balance of all coupling mechanisms (see Supporting Information).

Spin−orbit corrections for calculations of H−D coupling constants in heavy metal dihydrogen and dihydride complexes are not required at the present level of computational accuracy but will become important for computational methods that are able to deliver one more digit of accuracy. In selected cases, spin−orbit terms might be crucial in order to obtain the correct magnitude for small J(H−D) in heavy metal complexes even with methods of the same accuracy as employed here and in related studies.

In contrast to the rather small spin−orbit coupling effects, vibrational corrections should be included in all calculations of J(H−D) at the present level of accuracy to achieve a more realistic comparison with experiments. Vibrational corrections will also give access to the temperature dependence of the coupling constants. Work along these lines is currently pursued in our group.

Acknowledgment. We thank Dr. D. G. Gusev for making his optimized geometries for the metal complexes available to us prior to publication of ref 7. We thank the Center for Computational Research (CCR) at the University of Buffalo for support. J.A. acknowledges the donors of the American Chemical Society Petroleum Research Fund and the CAREER program of the National Science Foundation (CHE-0447321) for financial support of his research.

Supporting Information Available: Expanded versions of the data tables where the FC, PSO, and DSO contributions to the spin−spin coupling constants are listed separately. This material is available free of charge via the Internet at http://pubs.acs.org.

References

(1) Kubas, G. J. *J. Organomet. Chem.* **2001**, *635*, 37−68.

(2) Heinekey, D. M.; Luther, T. A. *Inorg. Chem.* **1996**, *35*, 4396−4399.

(3) Gelabert, R.; Moreno, M.; Lluch, J. M.; Lledos, A. *J. Am. Chem. Soc.* **1997**, *119*, 9840−9847.

(4) Gelabert, R.; Moreno, M.; Lluch, J. M.; Lledos, A.; Pons, V.; Heinekey, D. M. *J. Am. Chem. Soc.* **2004**, *126*, 8813−8822.

(5) Maltby, P. A.; Schlaf, M.; Steinbeck, M.; Lough, A. J.; Morris, R. H.; Klooster, W. T.; Koetzle, T. F.; Srivastava, R. C. *J. Am. Chem. Soc.* **1996**, *118*, 5396−5407.

(6) Gründemann, S.; Limbach, H.-H.; Buntkowsky, G.; Sabo-etienne, S.; Chaudret, B. *J. Phys. Chem. A* **1999**, *103*, 4752−4754.

(7) Gusev, D. *J. Am. Chem. Soc.* **2004**, *126*, 14249−14257.

(8) Göttger-Schnetmann, I.; White, P. S.; Brookhart, M. *Organometallics* **2004**, *23*, 1766−1776.

(9) Gelfand, I. M.; Fomin, S. V. *Calculus of Variations*; Dover: Mineola, NY, 2000.

(10) Ripmeester, J. A.; Ratcliffe, C. I. *Solid-state NMR studies of inclusion compounds*; National Research Council of Canada, Ottawa 1989.

(11) Conner Jr., W. C.; Falconer, J. L. *Chem. Rev.* **1995**, *95*, 759−788.

(12) Mao, W. L.; Mao, H.-K.; Goncharov, A. F.; Struzhkin, V. V.; Guo, Q.; Hu, J.; Shu, J.; Hemley, R. J.; Somayazulu, M.; Zhao, Y. *Science* **2002**, *297*, 2247−2249.

(13) Shen, K.; Pietrass, T. *Appl. Phys. Lett.* **2004**, *84*, 1567−1569.

(14) Züttel, A.; Wenger, P.; Sudan, P.; Mauron, P.; Orimo, S.-I. *Mater. Sci. Eng. B* **2004**, *108*, 9−18.

(15) Schlapbach, L.; Züttel, A. *Nature* **2001**, *414*, 353−358.

(16) Lueking, A. D.; Yang, R. T. *App. Catal. A* **2004**, *265*, 259−268.

(17) Rosi, N. L.; Eckert, J.; Eddaoudi, M.; Vodak, D. T.; Kim, J.; Keeffe, M. O.; Yaghi, O. M. *Science* **2003**, *300*, 1127−1129.

(18) Schreckenbach, G. *J. Chem. Phys.* **1999**, *110*, 11936−11949.

(19) Patchkovskii, S.; Autschbach, J. Manuscript in preparation.

(20) Autschbach, J. The calculation of NMR parameters in transition metal complexes. In *Principles and Applications of Density Functional Theory in Inorganic Chemistry I*; Kaltsoyannis, N., McGrady, J. E., Eds.; Springer: Heidelberg, 2004; Vol. 112.

(21) Autschbach, J. Calculation of heavy-nucleus chemical shifts: Relativistic all-electron methods. In *Calculation of NMR and EPR Parameters. Theory and Applications*; Kaupp, M., Bühl, M., Malkin, V. G., Eds.; Wiley-VCH: Weinheim, 2004.

(22) Autschbach, J.; Ziegler, T. Relativistic calculation of spin−spin coupling constants. In *Calculation of NMR and EPR Parameters. Theory and Applications*; Kaupp, M., Bühl, M., Malkin, V. G., Eds.; Wiley-VCH: Weinheim, 2004.

(23) Autschbach, J.; Ziegler, T. Relativistic Computation of NMR shieldings and Spin−spin Coupling Constants. In *Encyclopedia of Nuclear Magnetic Resonance*; Grant, D. M., Harris, R. K., Eds.; John Wiley & Sons: Chichester, 2002; Vol. 9.

(24) Bühl, M.; Kaupp, M.; Malkina, O. L.; Malkin, V. G. *J. Comput. Chem.* **1999**, *20*, 91−105.

(25) Bühl, M. *Chem. Phys. Lett.* **1997**, *267*, 251−257.

(26) Hieringer, W.; Görling, A.; Arbouznikov, A.; Kaupp, M. Manuscript to be submitted.

(27) Termaten, A. J.; Aktas, H.; Schakel, M.; Ehlers, A. W.; Lutz, M.; Spek, A. L.; Lammertsma, K. *Organometallics* **2003**, *22*, 1827−1834.

(28) Kaupp, M. Untersuchung der Strukturen, Energien und NMR-Eigenschaften von Übergangsmetallverbindungen mit Hilfe quantenchemischer Methoden, 1996 Habilitationsschrift, Universität Stuttgart, Germany.

(29) Kaupp, M.; Malkin, V. G.; Malkina, O. L. NMR of transition metal compounds. In *Encyclopedia of Computational Chemistry*; von Ragué Schleyer, P., Ed.; John Wiley & Sons: Chichester, 1998.

(30) Lichtenberger, D. L. *Organometallics* **2003**, *22*, 1599−1602.

(31) Autschbach, J.; Ziegler, T. *J. Am. Chem. Soc.* **2001**, *123*, 5320−5324.

(32) Craw, J. S.; Bacskay, G. B.; Hush, N. S. *J. Am. Chem. Soc.* **1994**, *116*, 5937−5948.

(33) Bacskay, G. B.; Bytheway, I.; Hush, N. S. *J. Am. Chem. Soc.* **1996**, *118*, 3753−3756.

(34) Helgaker, T.; Jaszuński, M.; Ruud, K. *Chem. Rev.* **1999**, *99*, 293−352.

(35) Helgaker, T.; Watson, M.; Handy, N. C. *J. Chem. Phys.* **2000**, *113*, 9402−9409.

(36) Sychrovský, V.; Gräfenstein, J.; Cremer, D. *J. Chem. Phys.* **2000**, *113*, 3530−3547.

(37) Autschbach, J.; Ziegler, T. *J. Chem. Phys.* **2000**, *113*, 936−947.

(38) Autschbach, J.; Ziegler, T. *J. Chem. Phys.* **2000**, *113*, 9410−9418.

(39) van Lenthe, E.; Baerends, E. J.; Snijders, J. G. *J. Chem. Phys.* **1993**, *99*, 4597−4610.

(40) van Lenthe, E. *The ZORA Equation*; Thesis, Vrije Universiteit Amsterdam, Netherlands, 1996.

(41) Fonseca Guerra, C.; Visser, O.; Snijders, J. G.; te Velde, G.; Baerends, E. J. Parallelisation of the Amsterdam Density Functional Program. In *Methods and Techniques for Computational Chemistry*; STEF: Cagliari, 1995.

(42) te Velde, G.; Bickelhaupt, F. M.; Baerends, E. J.; van Gisbergen, S. J. A.; Fonseca Guerra, C.; Snijders, J. G.; Ziegler, T. *J. Comput. Chem.* **2001**, *22*, 931−967.

(43) Baerends, E. J. et al. Amsterdam Density Functional, Theoretical Chemistry, Vrije Universiteit, Amsterdam, URL http://www.scm.com.

(44) Autschbach, J.; Ziegler, T. *J. Am. Chem. Soc.* **2001**, *123*, 3341−3349.

(45) Autschbach, J.; Igna, C. D.; Ziegler, T. *J. Am. Chem. Soc.* **2003**, *125*, 1028−1032.

(46) Autschbach, J.; Igna, C. D.; Ziegler, T. *J. Am. Chem. Soc.* **2003**, *125*, 4937−4942.

(47) Autschbach, J.; Le Guennic, B. *J. Am. Chem. Soc.* **2003**, *125*, 13585−13593.

(48) Ramsey, N. F. *Phys. Rev.* **1953**, *91*, 303−307.

(49) Pyykkö, P. *Theor. Chem. Acc.* **2000**, *103*, 214−216.

(50) Wolff, S. K.; Ziegler, T.; van Lenthe, E.; Baerends, E. J. *J. Chem. Phys.* **1999**, *110*, 7689−7698.

(51) Adamo, C.; Barone, V. *J. Chem. Phys.* **1998**, *108*, 664−675.

(52) Perdew, J. P.; Burke, K.; Wang, Y. *Phys. Rev. B* **1996**, *54*, 16533−16539.

(53) Burke, K.; Perdew, J. P.; Wang, Y. Derivation of a generalized gradient approximation: the PE91 density functional. In *Electronic density functional theory. Recent progress and new directions*; Dobson, J. F., Vignale, G., Das, M. P., Eds.; Plenum Press: New York, 1998.

(54) Vosko, S. H.; Wilk, L.; Nusair, M. *Can. J. Phys.* **1980**, *58*, 1200−1211.

(55) Becke, A. D. *Phys. Rev. A* **1988**, *38*, 3098−3100.

(56) Perdew, J. P. *Phys. Rev. B* **1986**, *33*, 8822−8824.

(57) Perdew, J. P.; Burke, K.; Ernzerhof, M. *Phys. Rev. Lett.* **1996**, *77*, 3865−3868.

(58) Zhang, Y.; Yang, W. *Phys. Rev. Lett.* **1998**, *80*, 890.

(59) Perdew, J. P.; Burke, K.; Ernzerhof, M. *Phys. Rev. Lett.* **1998**, *80*, 891.

(60) Hammer, B.; Hansen, L. B.; Norskov, J. K. *Phys. Rev. B* **1999**, *59*, 7413−7421.

(61) Schipper, P. R. T.; Gritsenko, O. V.; van Gisbergen, S. J. A.; Baerends, E. J. *J. Chem. Phys.* **2000**, *112*, 1344−1352.

(62) Gritsenko, O. V.; Schipper, P. R. T.; Baerends, E. J. *Int. J. Quantum Chem.* **2000**, *76*, 407−419.

(63) Chong, D. P.; Gritsenko, O. V.; Baerends, E. J. *J. Chem. Phys.* **2002**, *116*, 1760−1772.

(64) Grüning, M.; Gritsenko, O. V.; van Gisbergen, S. J. A.; Baerends, E. J. *J. Chem. Phys.* **2002**, *116*, 9591−9601.

(65) van Gisbergen, S. J. A.; Pacheco, J. M.; Baerends, E. J. *Phys. Rev. A* **2001**, *63*, 63201.

(66) Poater, J.; van Lenthe, E.; Baerends, E. J. *J. Chem. Phys.* **2003**, *118*, 8584−8593.

(67) Le Guennic, B.; Matsumoto, K.; Autschbach, J. *Magn. Res. Chem.* **2004**, *42*, S99−S116.

(68) Kowalewski, J. *Annu. Rep. NMR Spectrosc.* **1982**, *12*, 81−176.

(69) Ruden, T. A.; Lutnæs, O. B.; Helgaker, T.; Ruud, K. *J. Chem. Phys.* **2003**, *118*, 9572−9581.

(70) Light, J. C.; Hamilton, I. P.; Lill, J. V. *J. Chem. Phys.* **1985**, *82*, 1400−1409.

(71) Witek, H. A.; Fedorov, D. G.; Hirao, K.; Viel, A.; Widmark, P.-O. *J. Chem. Phys.* **2002**, *116*, 8396−8406.

(72) Koch, W.; Holthausen, M. C. *A Chemist's Guide to Density Functional Theory*, 2nd ed.; Wiley-VCH: Weinheim, 2001.

(73) Matveev, A.; Staufer, M.; Mayer, M.; Rösch, N. *Int. J. Quantum Chem.* **1999**, *75*, 863.

CT050042J